JGR Atmospheres

RESEARCH ARTICLE
10.1029/2024JD042682

Atmospheric Aerosols Versus Total Atmospheric Deposition in Guadeloupe (Lesser Antilles): Composition, Concentration, and Flux

Yangjunjie Xu-Yang[1,2], Rémi Losno[1], Céline Dessert[1], Fabrice Monna[3], Natalie M. Mahowald[4], and Mickael Tharaud[1]

[1]Université Paris Cité, Institut de Physique du Globe de Paris, CNRS UMR 7154, Paris, France, [2]Now at Laboratoire des Sciences du Climat et de l'Environnement (LSCE/IPSL), UMR 8212 (CEA-CNRS-UVSQ), Université Paris-Saclay, Gif-sur-Yvette, France, [3]Université de Bourgogne, UMR CNRS 6298, ARTEHIS, Dijon, France, [4]Department of Earth and Atmospheric Science, Cornell University, Ithaca, NY, USA

Key Points:

- Atmospheric aerosols and total atmospheric deposition are measured in the Caribbean region and compared with the model
- The modeled total deposition rate is underestimated, while model aerosol concentration is overestimated for near-ground dust and sea salt
- Dust and sea salt are washed more efficiently than predicted due to enhanced vertical motion, cloudiness, and precipitation on the island

Correspondence to:
Y. Xu-Yang,
yangjunjie.xu@lsce.ipsl.fr

Citation:
Xu-Yang, Y., Losno, R., Dessert, C., Monna, F., Mahowald, N. M., & Tharaud, M. (2025). Atmospheric aerosols versus total atmospheric deposition in Guadeloupe (Lesser Antilles): Composition, concentration, and flux. *Journal of Geophysical Research: Atmospheres*, *130*, e2024JD042682. https://doi.org/10.1029/2024JD042682

Received 12 OCT 2024
Accepted 16 MAR 2025

Author Contributions:
Conceptualization: Yangjunjie Xu-Yang, Rémi Losno, Céline Dessert, Fabrice Monna, Natalie M. Mahowald
Data curation: Yangjunjie Xu-Yang, Rémi Losno, Céline Dessert
Formal analysis: Yangjunjie Xu-Yang, Rémi Losno, Céline Dessert, Fabrice Monna, Natalie M. Mahowald
Funding acquisition: Rémi Losno, Céline Dessert
Investigation: Yangjunjie Xu-Yang, Rémi Losno, Céline Dessert, Fabrice Monna, Natalie M. Mahowald, Mickael Tharaud
Methodology: Yangjunjie Xu-Yang, Rémi Losno, Céline Dessert, Fabrice Monna, Natalie M. Mahowald, Mickael Tharaud

Abstract Atmospheric mineral dust deposition is an important source of nutrients for ocean and tropical island ecosystems. Direct deposition measurements are generally more reliable at local scale than dust deposition models, even those based on aerosol concentration measurements. Whatever the scale, relevant local observations are necessary for model evaluation. We present here the results obtained by direct measurement of atmospheric aerosols and total atmospheric deposition using a 14-month time series from the Caribbean region. Total deposition velocity, lifetime, and scavenging ratio of major and trace elements were determined. Comparing total deposition fluxes of aluminum (dust proxy) and sea-salt sodium (sea-salt proxy) with Community Atmosphere Model (CAM6) outputs shows that the modeled total deposition rate is underestimated by a factor of two for dust and by a factor of eight for sea salt, while model aerosol concentration is larger than concentration measured near ground level. This result is due to wet deposition being underestimated in the model. The scavenging ratio (w/w) of Saharan dust elements ranges from 95 to 1,390, with a median of 530, close to the geometric mean value of 513. Sea salt presents a greater range of scavenging ratio values, from 325 to 2,355, with a median of 1,180, close to the geometric mean value of 1,030. The lead isotope ratio $^{206}Pb/^{207}Pb$ clearly highlights differences in lead origin between aerosols and deposits, revealing that aerosol samples are enriched by anthropogenic sources.

Plain Language Summary Atmospheric aerosols are particles suspended in the air, from sea spray (sea salt), from dry soil (dust), volcanoes (ash), plants (e.g., pollen), and human activity (pollution). Dust is transported by wind, then falls to the ground (dry deposition) or is brought down by rain (wet deposition). Based on 14 months of measurements in the Guadeloupe Islands (Lesser Antilles), we describe the relationship between the aerosols suspended in the air and their deposition, both dry and wet. The models describing the behavior of atmospheric aerosols predict high concentrations in the air and a fairly slow total deposition rate, especially in the form of dry deposition. The results of our study demonstrate the opposite: in the case of the tropical island of Guadeloupe, the total atmospheric deposition fluxes are predominantly governed by wet deposition, leaving a very short residence time for atmospheric aerosols traveling close to the ground before they are brought down. We therefore measure low aerosol concentrations remaining in the air close to ground level. We highlight little-known phenomena of atmospheric aerosol scavenging close to the ground.

1. Introduction

Aerosols contribute to the Earth's radiation budget (Bellouin et al., 2020) and also to biogeochemical cycles; both these factors impact the Earth's climate. Biogeochemical studies from around the world have suggested that aerosol particles bring significant nutrients into ecosystems once deposited on land (Abouchami et al., 2013; Chadwick et al., 1999; Dessert et al., 2015, 2020; Kennedy et al., 1998; McClintock et al., 2015, 2019; Pett-Ridge, Derry, & Barrows, 2009; Pett-Ridge, Derry, & Kurtz, 2009; Yu et al., 2015). Dessert et al. (2020) and Xu-Yang et al. (2022) emphasize the crucial role that atmospheric particles (including Saharan dust and marine aerosols) play in fertilizing tropical rain forests. Dust deposited in oceans also has a strong potential impact on biogeochemical processes, as shown in Cipolloni et al. (2024) and Dassié et al. (2022) for floating holopelagic Sargassum and in Pabortsava et al. (2017) and Guerreiro et al. (2017, 2023) for plankton, with Fe as the most important limiting nutrient for open ocean biota (e.g., Jickells, 2005; Mahowald et al., 2011).

Project administration: Rémi Losno, Céline Dessert
Resources: Rémi Losno, Céline Dessert
Software: Fabrice Monna
Supervision: Rémi Losno, Céline Dessert
Validation: Yangjunjie Xu-Yang, Rémi Losno, Céline Dessert, Fabrice Monna, Mickael Tharaud
Visualization: Yangjunjie Xu-Yang, Rémi Losno, Céline Dessert, Fabrice Monna
Writing – original draft: Yangjunjie Xu-Yang, Rémi Losno, Céline Dessert, Fabrice Monna, Natalie M. Mahowald
Writing – review & editing: Yangjunjie Xu-Yang, Rémi Losno, Céline Dessert, Fabrice Monna, Natalie M. Mahowald, Mickael Tharaud

Dust models are widely used to study dust transport at a global scale (e.g., Jickells, 2005; Mahowald et al., 2006). Measured data points can be complemented by model-based deposition maps to provide continuous spatial coverage (Vet et al., 2014). Large differences exist between models because of large differences in emission, transport, and deposition processes within the models (Huneeus et al., 2011; Shao et al., 2011). Models are generally evaluated by comparison with various types of measured data, which can serve to test specific model modules (Mahowald et al., 2006). As measuring atmospheric deposition is difficult, very few data are available; models are therefore rarely checked against deposition flux data. For this reason, models are often tested using indirect measurements, including aerosol optical depth measured by satellite (Holben et al., 2001), but are rarely tested with direct field data (Prospero et al., 2010). Total atmospheric deposition is thus computed using dry deposition velocity to calculate dry deposition flux, while scavenging ratio is used to calculate wet deposition flux (Duce et al., 1991; Mahowald et al., 2006, 2011, 2014; Vet et al., 2014). Scavenging ratios and deposition velocities are critical parameters in atmospheric transport models, while lifetime is an important diagnostic value that can be calculated from model output (Mahowald et al., 2014). The scavenging of particles, including their chemical constituents, has so far been rarely documented worldwide (Kulshrestha et al., 2009). Scavenging ratio postulates that the partition between the suspended aerosol and the precipitating water is constant (e.g., Galloway et al., 1993; Kulshrestha et al., 2009; Tegen & Fung, 1994). The wet deposition flux is therefore proportional to the aerosol load in the atmospheric column that can be scavenged during each rain event; it also depends on the vertical distribution of rain versus that of dust (Tegen & Fung, 1994). Aerosol lifetime is used to estimate how fast aerosols are removed from the atmosphere; it is closely related to deposition velocity. Wet deposition of aerosols is associated with precipitation, whereas dry deposition includes diffusion, turbulent collision of aerosols with the surface, and gravitational settling. Many uncertainties are linked to these processes, resulting in large uncertainties in model estimates of aerosol lifetimes (Mahowald et al., 2011). Deposition fluxes predicted by different models have been shown to vary by one order of magnitude because of discrepancies between these parameters (Huneeus et al., 2011). Furthermore, using surface dust concentration to infer atmospheric dust deposition can introduce large uncertainties, even though the near-surface concentration of dust is correctly measured (e.g., Giardina & Buffa, 2018; Klug & Communities, 1992; Mahowald et al., 2006). For example, when aerosols are carried above the boundary layer, aerosol particles contained in rainwater originate from high altitude and not from near the surface, as identified in the Kerguelen Islands (Southern Ocean) by Heimburger et al. (2012). In this case, surface aerosols are not representative of aerosols scavenged by rain.

Previous studies have been published on Saharan dust aerosols and deposits collected across the equatorial North Atlantic, below the dust plume core, based on subsurface sediment traps for deposition collection and shipboard aerosol collection (Korte et al., 2016, 2017, 2020; Van Der Does et al., 2018, 2020, 2021). A downwind change in the mineralogical composition, radiogenic isotopes, trace and major elemental compositions have been observed in Saharan dust collected by sediment traps along this Atlantic Ocean transect (Korte et al., 2016, 2017; Van Der Does et al., 2018). Chemical composition differences between aerosols and deposition are reported across the equatorial North Atlantic Ocean (Van Der Does et al., 2018). However, synchronous time series directly linking aerosol and deposition have never been studied in the Tropical North Atlantic Ocean. In this article, we present the results of a 14-month experiment (from March 2017 to May 2018) in the Guadeloupe Islands, where total atmospheric deposition fluxes and atmospheric aerosol concentrations were measured synchronously on a weekly basis. We address two major questions: (a) How do scavenging ratio, lifetime, and deposition velocity vary? (b) How do our results compare with previous studies conducted on aerosols in the Tropical North Atlantic Ocean region?

2. Material and Method

2.1. Sampling

Total atmospheric deposition and aerosols were sampled continuously during an integration period ranging from 5 to 15 days at the remote site of OVSG (Observatoire Volcanologique et Sismologique de Guadeloupe, Gourbeyre, Guadeloupe, 15°58′50″N, 61°42′13″W, altitude: 411 m; Figure 1). Total atmospheric deposition was sampled from 02 March 2015 to 03 August 2018, on the roof of a building, 8 m above the ground. Details on deposition sampling are provided in Xu-Yang et al. (2022).

Atmospheric aerosols were sampled simultaneously in the vicinity of the deposition collector by aspiration of ambient air through a membrane filter (47 mm diameter, 0.45 μm porosity) from 27 March 2017 to 28 May 2018.

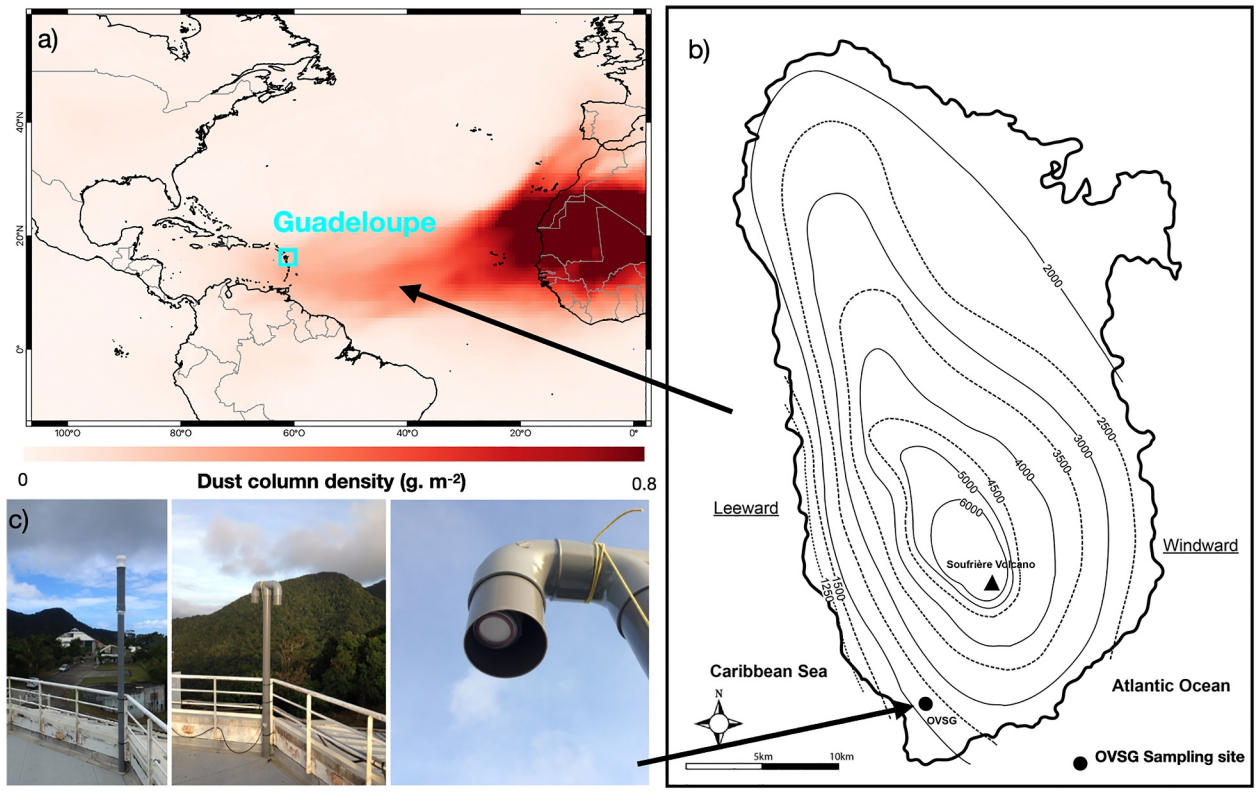

Figure 1. Sampling site in Guadeloupe. (a) Dust event observed between 19 June 2017 and 28 June 2017, showing Guadeloupe inside the transatlantic dust plume. Color scale corresponds to the estimated averaged dust concentration during this period, calculated using satellite measurements and the MERRA-2 model proposed by Giovanni NASA EarthData (https://giovanni.gsfc.nasa.gov/giovanni/, Beaudoing et al., 2020) (b) Isohyet map of Basse-Terre Island, Guadeloupe. (c) Photos of the sampling systems. Total atmospheric deposition (left), aerosol filtration (middle), and view of aerosol filtration from below (right).

Only the 14-month period during which aerosols and deposition were sampled simultaneously is discussed in this article. Membrane filters were washed with ultrapure diluted hydrochloric acid solution and rinsed with ultrapure water prior to the sampling campaign. Two types of filters were used (both Whatman™): mixed cellulose ester at the beginning of the time series and polycarbonate at the end, because some of the previously washed mixed cellulose filters lost their mechanical properties in the hot and humid tropical atmosphere of Guadeloupe. Air was drawn through a filter for approximately 7 days using a pump with a flow rate of 11 L min^{-1}. The volume of air that passed through each filter was recorded using a Gallus 2000 (Schlumberger™) volumetric gas meter connected to the outlet of the pump. The open-face filter holder was placed facing downwards 2 m above the flat roof of the building, protected by a section of PVC tube, 80 mm in diameter. All filter manipulations were protected either by a box under a flow of ultraclean air (HEPA 14 filter) in the field, or by the ISO-5 cleanroom in the laboratory.

To assess contamination in the field, field blanks (aerosol filters and deposition bottles) were prepared following the same protocols.

The filter used to collect aerosols was generally renewed more frequently than the bottle used to collect total deposition. One deposition sample can therefore be paired with the pooled aerosol sample by merging the filters collected during the corresponding deposition sampling period.

2.2. Digestion of Aerosol Samples

All the sampling materials used in this study were carefully cleaned with acid and Milli-Q water in order to minimize possible contamination from the devices. After sampling, the filters coated with collected aerosols were brought back to the laboratory for complete digestion using PTFE vessels, in a mixture of sub-boiled HNO_3/HF (9:1), on a heater plate at 125°C for 18 hr, and then evaporated at the same temperature. The evaporation residue

was dissolved using 3 mL of 30% nitric acid solution and diluted to 60 mL with ultrapure water for analyses (see Xu-Yang et al. (2021), for details). To assess contamination during digestion, digestion blanks were prepared following the same digestion protocol.

2.3. Chemical Analysis of Trace and Major Elements

Major and minor elements (Al, Ba, Ca, Fe, Li, Mg, Mn, P, S, Sc, Sr, and Ti) were determined using an ARCOS (Spectro-Ametek) ICP-AES, equipped either with a CETAC ultrasonic nebulizer, or with a concentric nebulizer coupled to a cyclonic chamber. The ICP-AES was calibrated by measuring a set of multi-elementary solutions, with concentrations between 0 and 500 µg L^{-1}. The calibration intercept was computed as the average of eight blank replicates. Trace elements (As, Be, Cd, Co, Cu, Mo, Ni, Pb, Rb, Se, Tl, U, V, and Rare Earth Elements [REEs]) were determined using a Thermo Element 2 (FS-HR-ICP-MS), equipped with a concentric micro-nebulizer coupled to a cyclonic chamber. High-resolution analysis avoids polyatomic interference for elements lighter than arsenic, and also for REEs (Heimburger et al., 2013). The FS-HR-ICP-MS was calibrated with fourteen blank replicates and five replicates of a 1 µg L^{-1} multi-elementary solution. Flame photometry (ColeParmer 360) was used for Na and K measurement, with linear calibration between 0 and 50 mg L^{-1} for K, and polynomial (2nd degree) calibration between 0 and 50 mg L^{-1} for Na, to take into account auto-absorption of Na atoms for the higher concentrations.

Each detection limit (analytical, digestion, and field) was calculated as three times the standard deviation of the respective blanks. The median values for blank aerosol filters were under the analytical detection limit for Li, Sc, Mn, Be, Mo, Cd, Tl, U, Se, Sm, Eu, Tb, Ho, Tm, and Lu in the polycarbonate filters; and for Li, Sc, Be, Cd, U, Tm, Yb, Lu in the mixed cellulose ester filters. For all these elements, as the digestion and field detection limits were equal to the analytical detection limit, no field blank correction was applied. For each of the other elements, a field blank correction was applied by subtracting the median quantity measured in the field blank filters (Table A1).

Elemental analysis of total deposition samples is detailed in Xu-Yang et al. (2022). The three detection limits were obtained in the same way as the aerosol detection limits. The median quantities found in field blanks were under the detection limit for Li, Mn, Sc, Sr, Be, Mo, Cd, Sb, Tl, U, Ni, Se, Gd, Tb, Ho, Tm, Lu, so that no blank correction was made for these elements. For these elements, the two other detection limits are equal to the analytical detection limit. For each of the other elements, a blank correction was applied by subtracting the median quantity found in field blanks; the field detection limit was used instead of the analytical detection limit.

The elemental concentrations in air, $[X]$ (ng m^{-3}), were calculated by dividing the quantity of element X found on a filter, $Q_X(sample)$ (ng), possibly corrected from field blanks, $Q_X(blank)$, by the volume of air, V_{air} (m^3), that passed through the filter during the sampling, using Equation 1.

$$[X] = \frac{Q_X(sample) - Q_X(blank)}{V_{air}} \quad (1)$$

For each sample, the elemental total deposition fluxes, $F(X)_{total}$, for an element X were calculated by dividing the measured quantity of element X, $Q_X(sample)$, possibly corrected from field blanks, $Q_X(blank)$, by the aperture area of the funnel, $S_{funnel} = 0.0113$ m^2, and by the exposition time, $T_{exposure}$ (d), using Equation 2.

$$F(X)_{total} = \frac{Q_X(sample) - Q_X(blank)}{S_{funnel} \times T_{exposure}} \quad (2)$$

2.4. Lead Isotope Analysis

Lead isotopes ^{206}Pb and ^{207}Pb were measured using the Element 2 FS-HR-ICP-MS. A loss of linearity was observed for counting rates higher than 600,000 cps, corresponding to a lead concentration of 1 µg L^{-1}. Samples where the lead concentration was too high were diluted to around 0.5 µg L^{-1} before analysis. A correction was applied to raw measured ratios using the NBS 981 lead isotope standard (1.0933 for $^{206}Pb/^{207}Pb$), verified by MAG-1 and STM-1 geostandard measurements (Table A3).

The median lead quantity in field blanks was equal to 0.4 ng for cellulose nitrate filters, 1.8 ng for polycarbonate filters, and 0.5 ng for total deposition samples. As the quantity of lead in the cellulose nitrate filter blanks and total

deposition blanks was always less than 1% of the total quantity of lead measured in the respective sample series, correcting their isotope ratios from the blanks was not necessary. As the quantity of lead in the polycarbonate filter blanks was higher, the isotope ratio had to be corrected from the blanks. The measured average $^{206}Pb/^{207}Pb$ ratio was 1.169; for the 19 aerosol samples collected on polycarbonate filters, the maximum blank correction of 0.003 was applied to 1 sample, a correction equal to or less than 0.0002 was applied to 10 samples, with no correction for the other 8 samples.

2.5. Determination of Saharan Dust and Sea Salt

The total deposition mass flux of Saharan dust, $F(dust)_{total}$, was estimated assuming a pure Saharan origin of aluminum, using Equation 3:

$$F(Al)_{total} = F(dust)_{total} \times wt\%_{Al,crust\ model}\ F(dust)_{total} = \frac{F(Al)_{total}}{wt\%_{Al,crust\ model}} \tag{3}$$

where $wt\%_{Al,crust\ model}$ is the aluminum model composition equal to 8.15%, as in Rudnick and Gao (2014). The Saharan dust concentration in air was calculated in the same way, using aluminum concentration in air, instead of aluminum flux.

The total deposition mass flux of sea salt, $F(sea\ salt)_{total}$, was estimated using the model proposed in Brewer (1975), assuming that sea salt and dust were the only sources of the sodium deposition flux. Sea-salt sodium was first deduced from total sea salt using Equation 4, as proposed by Rahn (1976):

$$Na_{sea\ salt} = Na_{total} - Na_{custal} = Na_{total} - Al\left(\frac{Na}{Al}\right)_{crust\ model} \tag{4}$$

and then sea-salt flux was calculated using Equation 5:

$$F(sea\ salt)_{total} = \frac{F(Na_{sea\ salt})}{wt\%_{Na,sea\ salt\ model}} \tag{5}$$

where $wt\%_{Na,sea\ salt\ model}$ is equal to the sodium mass fraction in sea salt: 30.6%. The concentration of sea salt in air is calculated in the same way.

2.6. Deposition Velocity, Scavenging Ratio, and Lifetime Calculation

The total deposition flux of X, $F(X)_{total}$, is expressed as the product of air concentration, $[X]_{air}$, times deposition velocity, $v(X)$, with Equation 6:

$$F(X)_{total} = [X]_{air} \times v(X) \Rightarrow v(X) = \frac{F(X)_{total}}{[X]_{air}} \tag{6}$$

As proposed for example, in Heimburger et al. (2012), wet deposition was calculated by subtracting dry deposition from total deposition. The dry deposition flux $F(X)_{dry}$ of a species X was deduced from dry deposition velocity $v_{dry\ deposition}$, and surface aerosol concentration of X in air $[X]_{air}$, with Equation 7.

$$F(X)_{dry} = [X]_{air} \times v_{dry\ deposition} \tag{7}$$

We assumed a dry deposition velocity of 0.3 cm s^{-1}, as proposed by L. Li et al. (2022) for our location; this value is also consistent with values estimated for Saharan dust in Florida (Prospero et al., 2010).

The wet deposition fluxes for element X were deduced by subtracting computed dry deposition from observed total deposition, with Equation 8:

$$F(X)_{wet} = F(X)_{total} - F(X)_{dry} \tag{8}$$

The wet deposition of a chemical species X is often parameterized with a dimensionless number, the scavenging ratio, $W_{mass}(X)$, which represents the partitioning of X between the same mass of rainwater and near-surface air, as in Equation 9:

$$W_{mass}(X) = \frac{[X]_{rain\ water}}{[X]_{air}} \frac{\rho_{air}}{\rho_{water}} \tag{9}$$

where $[X]_{rain\ water}$ and $[X]_{air}$ are the concentrations of the species X, respectively, in rainwater and in air, expressed in the same unit, and ρ_{water} and ρ_{air}, the densities of water and air, respectively, equal to 1,000 and 1.225 kg m^{-3}. Wet deposition flux was therefore expressed as a function of scavenging ratio $W_{mass}(X)$ and precipitation rate, PR (Equations 10 and 11):

$$F(X)_{wet} = [X]_{air} \times W_{mass}(X) \times \frac{\rho_{water}}{\rho_{air}} \times PR \tag{10}$$

giving

$$W_{mass}(X) = \frac{F(X)_{total} - F(X)_{dry}}{[X]_{air} \cdot PR} \times \frac{\rho_{air}}{\rho_{water}} \tag{11}$$

Note that if $[X]_{air}$ is expressed in μg m^{-3}, fluxes in μg m^{-2} d^{-1}, PR should be expressed in m d^{-1} to comply with the expression of $W_{mass}(X)$. As assumption of dry deposition velocity is uncertain, consequently affecting dry deposition flux calculation, the scavenging ratio was not calculated if the assumed dry deposition flux was larger than 40% of the measured total deposition flux. Among the 37 paired samples, no more than 3 were discarded for all the elements, except for phosphorus. This element was often below the aerosol detection limit, so only 3 paired samples could be retained for scavenging ratio calculation.

Lifetime for species X depends on the thickness of the atmospheric layer taken into account. Lifetime was deduced from deposition velocity $v(X)$, and the thickness of the layer above the ground h, using Equations 12 and 13:

$$Lifetime(X) = \frac{h}{v(X)} \tag{12}$$

giving

$$Lifetime(X) = \frac{[X]_{air}}{F(X)_{total}} \times h \tag{13}$$

2.7. Compositional Data Analyses (CoDA): Perturbation Diagram

Appropriate mathematical tools must be used to handle compositional data. Briefly, the suitable sample space of any compositional vector $\mathbf{x}$, representing a D-part subset of a whole $\mathbf{x} = [x_1, \ldots, x_D]$, is the simplex S^D, as defined in Aitchison (1982, 1986). It is particularly well adapted to situations where elemental ratios are more relevant than absolute values.

Let $\mathbf{x} = [x_1, \ldots, x_D]$ and $\mathbf{y} = [y_1, \ldots, y_D]$ denote two compositional vectors in S^D. Then $\mathbf{z}$, corresponding to the perturbation of $\mathbf{x}$ by $\mathbf{y}$, in S^D is given by Equation 14:

$$\mathbf{z} = \mathbf{x} \oplus \mathbf{y} = C[x_1 y_1, \ldots, x_D y_D] \tag{14}$$

with C the closure-to-unity operation defined as

$$C[\mathbf{x}] = \left[\frac{x_1}{\sum_{i=1}^{D} x_i}, \ldots, \frac{x_D}{\sum_{i=1}^{D} x_i} \right] \tag{15}$$

The neutral element of the perturbation is $\mathbf{e} = C[1,\ldots,1] = \left[\frac{1}{D},\ldots,\frac{1}{D}\right]$, and $\mathbf{x} = \mathbf{x} \oplus \mathbf{e}$, while the perturbation vector expressing compositional change from $\mathbf{y}$ to $\mathbf{x}$, noted $\mathbf{x} \ominus \mathbf{y}$, is equal to $\mathbf{x} \oplus \mathbf{y}^{-1}$, with $\mathbf{y}^{-1} = C\left[y_1^{-1},\ldots,y_D^{-1}\right]$. This representation is particularly relevant for showing REE profiles because no external normalization is necessary to conclude about the variability of these profiles.

Perturbation plots were made using the "compositions" package of R software (R Core Team, 2018), which was specifically designed to analyze compositional data (van den Boogaart & Tolosana-Delgado, 2013). More details on perturbation diagrams and compositional data analysis (CoDA) applied to atmospheric aerosol measurements are presented in Xu-Yang et al. (2021).

2.8. Model

Simulations of dust transported to Guadeloupe were conducted using the Community Atmosphere Model (CAM6), part of the Community Earth System Model (Danabasoglu et al., 2020). The model includes a modal description of aerosols (Liu et al., 2012, 2016). In such models, dust aerosols are generated in dry, unvegetated areas with strong winds, and then transported and deposited within a 3-dimensional transport framework (Albani et al., 2014; Kok et al., 2014; L. Li et al., 2022; Zender, 2003). A new dry deposition scheme was used for this set of simulations (L. Li et al., 2022; Petroff & Zhang, 2010). The model framework for this study was compared to available observations in several studies (Brodsky et al., 2023; L. Li et al., 2022; Mahowald et al., 2024). Models have difficulty matching the available AOD (Aerosol Optical Depth), concentration, and deposition data (Albani et al., 2014; Huneeus et al., 2009), and this model works in a similar way to other dust models.

3. Results and Discussion

3.1. Aerosol Concentration and Total Atmospheric Deposition Flux Measurement

Figure 2 shows atmospheric concentration and total atmospheric deposition flux variations for aluminum (dust proxy) and sea-salt sodium during the field experiment period. Aluminum atmospheric concentration varies between 0.02 and 5.45 μg m^{-3} (median value of 0.43 μg m^{-3}), with a higher concentration in summer (May–September 2017) revealing seasonal variation. Sea-salt sodium atmospheric concentration, calculated using Equation 4, varies between 0.8 and 5.2 μg m^{-3}, with the median value equal to 2.8 μg m^{-3}, with no obvious seasonality. In the same way, a seasonally higher total deposition rate is observed during summer for dust, while much less seasonal variability is visible for the total deposition rate of sea salt (as already shown in Xu-Yang et al. (2022)). No systematic similarities are observed between the aerosol concentration and total deposition flux patterns, whether for dust or sea salt. In the Caribbean region, the vertical distribution of dust was similar to the Saharan Air Layer transport (Dulac et al., 2001; Groß et al., 2016; Reid et al., 2003; Weinzierl et al., 2017). In the study of a single dust event in February at the same latitude over the Cape Verde Islands, Dulac et al. (2001) observed that 90% of the dust is transported at high altitude, above the marine boundary layer. At 950 m in altitude, the dust concentration may be 20 times higher on average than at ground level. During June and July 2000 in Puerto Rico, the maximum concentration of dust was observed at an altitude of 4,500 m (Reid et al., 2003). This is consistent with other recent studies conducted between June and July 2013 in Barbados, where dust concentration was found to be twice as large at an altitude of 2,800 m than at ground level (Groß et al., 2016; Weinzierl et al., 2017). The concentrations of other aerosol species have also been found to be variable at different altitudes (Groß et al., 2016; Weinzierl et al., 2017). Concentration measurements at surface level are thus not truly representative of the total atmospheric column nor of the marine boundary layer. Using aerosol concentration to estimate total deposition flux is therefore not straightforward.

3.2. Deposition Velocity and Lifetime for Saharan Dust, Sea Salt, and Elements

We computed the total deposition velocity (Figure 3), lifetime (for $h = 66$ m, Figure 3), and scavenging ratio (Figure 4), for each period and each measured element (Section 2.6). Both deposition velocity and lifetime for the paired samples (aerosol/deposit) vary substantially. This result shows that the deposition flux could not be accurately calculated by multiplying the aerosol concentration by a constant deposition velocity value.

The median values for total deposition velocity are very close for all the elements measured. The highest median deposition velocity is observed for sea salt (6.0 cm s^{-1}) and sodium (5.8 cm s^{-1}). The lowest median deposition velocity is observed for phosphorus (0.1 cm s^{-1}) and selenium (1.5 cm s^{-1}). Most of the remaining elements have

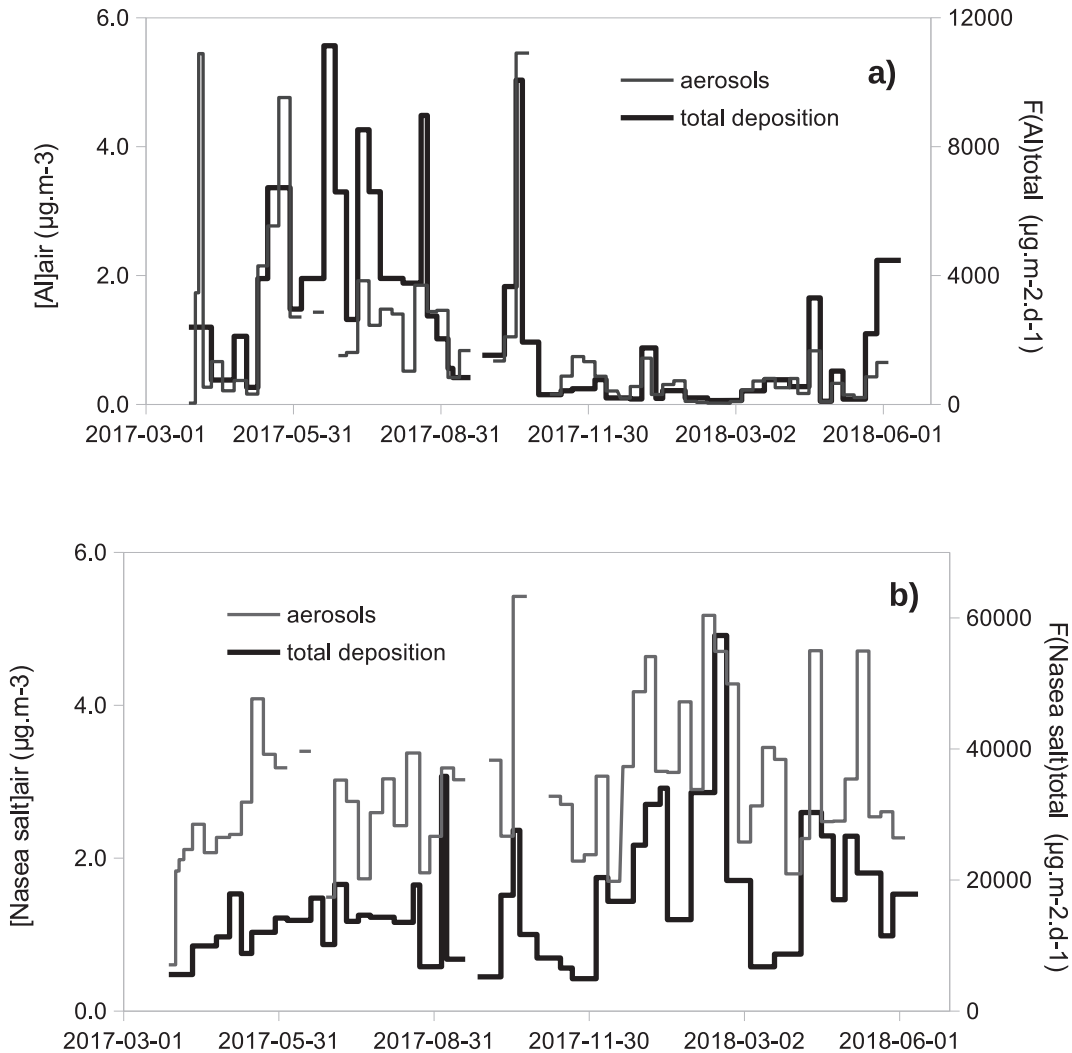

Figure 2. Atmospheric concentration and total deposition flux during the field experiment, for aluminum (a, dust proxy), and for sea-salt sodium (b, sea-salt proxy). Six aerosol samples were lost: 26 June 2017 to 28 June 2017, 24 October 2017 to 06 November 2017 and 18 December 2017 to 20 December 2017 (power outage), 18 September 2017 to 09 October 2017 (Maria storm), 05 June 2017 to 12 June 2017 and 19 June 2017 to 26 June 2017 (torn filters).

a median deposition velocity between 2 and 5 cm s^{-1}, in good agreement with the bulk deposition velocity of 2,400 m day^{-1} (2.8 cm s^{-1}) proposed in Kadko et al. (2015) for northern tropical oceans. Phosphorus has the lowest deposition velocity (median value equal to 0.1 cm s^{-1}) probably due to its local biogenic origin, as pointed out by Xu-Yang et al. (2022). Phosphorus is carried by insects, vegetable debris, and pollen, which are locally emitted and therefore with higher concentrations at ground level. For example, Raynor (1974) and Dong et al. (2019) measured a deposition velocity around 0.1 cm s^{-1} for pollen and vegetable debris, which is consistent with the observed range of deposition velocity for phosphorus.

For all elements except phosphorus, the total deposition velocity (between 2 and 5 cm s^{-1}) is much larger than the estimated dry deposition velocity (0.3 cm s^{-1}), implying that wet deposition is the major atmospheric deposition pathway. Consequently, the wet deposition lifetime is much shorter than the dry deposition lifetime.

3.3. Scavenging Ratio

Factors known to affect the scavenging ratio include the size of the particles being scavenged, their chemical composition, and cloud properties (including droplet size, temperature, and cloud type), with particle size distribution being the most important factor influencing the scavenging ratio (Cheng et al., 2021; Mahowald

et al., 2011, 2014). Aerosol scavenging is produced by a complex combination of numerous processes. However, many models estimate wet aerosol scavenging using the scavenging ratio as a simple parameter ranging between 400 and 1,000. Scavenging ratios computed with the field measurements (as described in Section 2.6) are plotted in Figure 4. The scavenging ratio for aluminum ranges from 95 to 1,390, with a geometric mean value of 513 and a median value of 530. Sodium levels range from 327 to 2,190, with a geometric mean value of 1,030 and a median value of 1,160. For most of the elements, scavenging ratios and the range of their variation measured during this study are consistent with values in the literature (Cheng et al., 2021) from other parts of the world.

The measured scavenging ratios are systematically higher for marine elements (sea salt) than for crustal elements (dust). Elements with high solubility present in coarse particles tend to have a higher scavenging ratio than elements with low solubility in fine particles (Cheng et al., 2021). As the sampling site is situated in the sea-salt emission zone, sea-salt particles are expected to be of coarser size than long-range transported dust particles (Kandler et al., 2018). A large proportion of the sodium, calcium, strontium, and magnesium is associated with the soluble, rather coarse sea-salt particles (Kandler et al., 2018; Xu-Yang et al., 2022); these elements therefore have a higher scavenging ratio than the other elements (Murphy et al., 2019). Scandium and aluminum are mainly associated with the poorly soluble dust particles, which are smaller in size than the sea-salt particles. As shown in Xu-Yang et al. (2022), phosphorus is associated with locally produced biogenic debris, which explains the low scavenging ratio observed. Selenium can be found in the gas phase in marine environments (Amouroux et al., 2001), explaining its low scavenging ratio, a result consistent with other studies (e.g., around 300 in Slinn et al. (1978)).

There is great variation in scavenging ratios from one sampled event to another. For all the measured elements, the median value of scavenging ratios ranges from 500 to 1,000, close to the constant value of the scavenging ratio used in simple deposition models ($W_{mass} = 750$; e.g., in Tegen et al. (2002) and Luo et al. (2003)). Thus, in the Guadeloupe Islands, an average total deposition flux of dust over long periods could be obtained with reasonable accuracy using such simple models. However, because of the strong variability observed, the constant value of the scavenging ratio cannot be used for a single event or for a short period, where the averaging effect cannot be invoked. In such cases, it is necessary to use models including more physically based parameterizations to calculate wet deposition, based on the vertical distribution of dust concentration and precipitation formation (Rasch et al., 2001).

3.4. Model Outputs and Comparisons

It is well known that precipitation, cloudiness, and fog strongly impact the process of aerosol removal and thus lifetimes (Mahowald et al., 2014; Tegen & Fung, 1994). In model estimates of lifetimes, gravitational settling lets the dust move down into the layers where wet deposition (clouds, precipitation, and fog) removes particles from the atmosphere (Mahowald et al., 2014, 2024). In the Southern Ocean, around the Kerguelen Islands, Heimburger et al. (2012) already observed that aerosols are almost totally scavenged in the lower atmospheric layers, including the boundary layer. The precipitation rate used by the model for the Guadeloupe sampling site is 475 mm yr^{-1}. The precipitation rate measured on-site in Guadeloupe for 2016 was 1,800 mm yr^{-1}, four times higher than the rate in the model, while the precipitation rate measured for 2017 was 3,600 mm yr^{-1}, 8 times higher. The precipitation recorded on-site during this study is consistent with long-term observations published by Chaperon et al. (1985). As pointed out by Albani et al. (2014), the model overestimates near-ground dust and sea-salt aerosol concentration (Table 1), because it underestimates precipitation. The model also overestimates dry deposition flux because it overestimates aerosol concentration. The wet deposition lifetime is therefore much larger (x10) in the model than the observed value, while the total deposition flux is underestimated by a factor of two.

Models do not accurately take into account the vertical motion in the lower layers over islands, where turbulence is much higher than over the open ocean (Albani et al., 2014; Cécé et al., 2014). Turbulence can enhance the downward vertical motion of aerosols and the upward vertical motion of water; the orographic effect can produce fog and cloud condensation by adiabatic cooling. Cloud droplets interact strongly with atmospheric aerosols and enhance their scavenging (J. Li et al., 2017). These small-scale phenomena associated with islands are normally neglected by global models, which generally give the same prediction for the Guadeloupe Islands and the open ocean. In the CAM simulations used here over Guadeloupe, cloud and fog events in the bottom model layer are rare, while frequent fog events are observed almost every day at the sampling site. The Guadeloupe Islands are

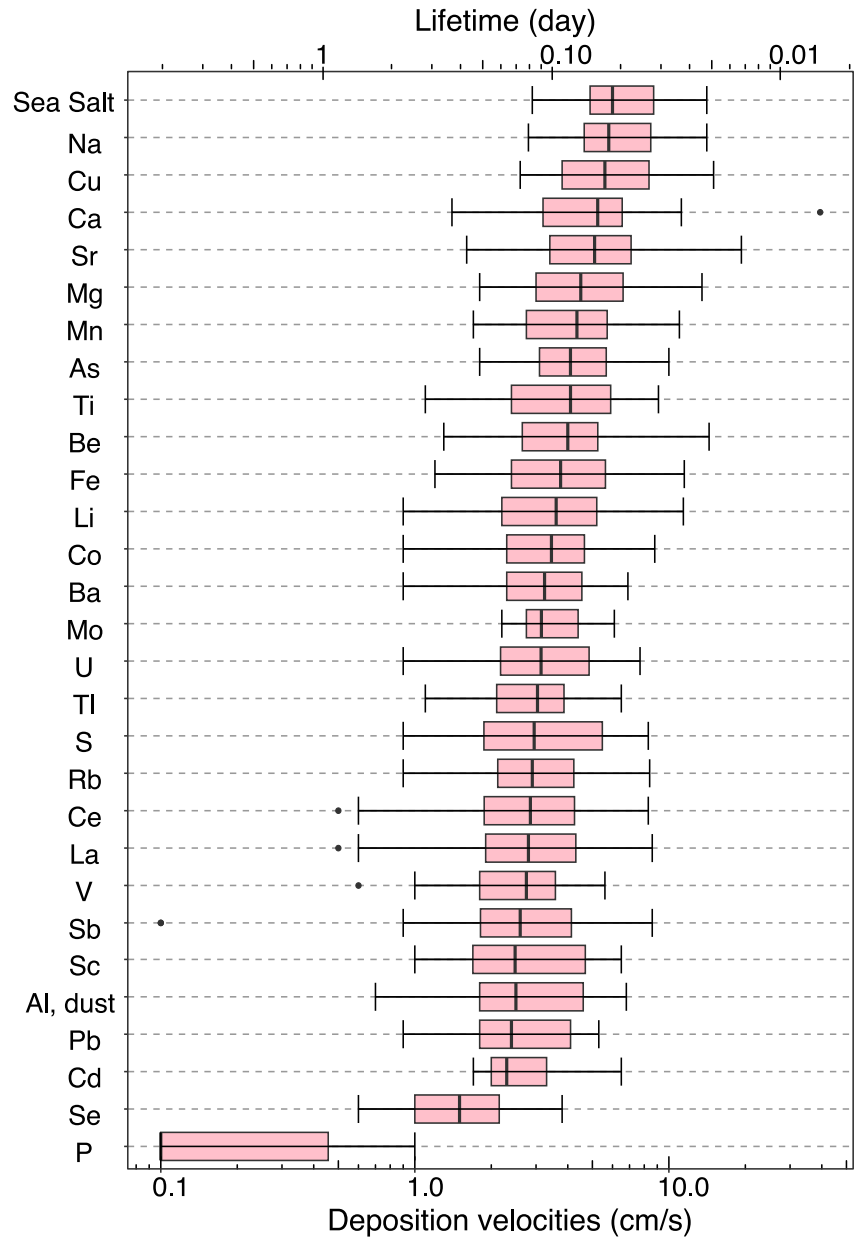

Figure 3. Deposition velocity (cm s^{-1}) and lifetime (day), with a 66 m atmospheric layer thickness for elements, dust (identical to Al), and sea salt (identical to sea-salt sodium).

situated in the storm tracks (Mahowald et al., 2011), thus enhancing the vertical movement of air, resulting in rapid removal of aerosols.

In conclusion, tropical islands such as Guadeloupe are characterized by thermal and orographic forcing, which may generate micro-scale air mass circulations, resulting in enhanced vertical motion, cloudiness, and precipitation. Thus, dust and sea salt are washed out more efficiently, resulting in a lower quantity of atmospheric aerosols compared to the predictions of global models.

3.5. Compositional Difference Between Aerosols and Total Deposition

The perturbation diagram between aerosols and total deposition is plotted in Figure 5, with all major and trace elements, except P, Sc, Be, Tl, and U, for which values lower than the detection limit were found for some samples, preventing a compositional data calculation with these elements. Marine elements, such as Na and Mg,

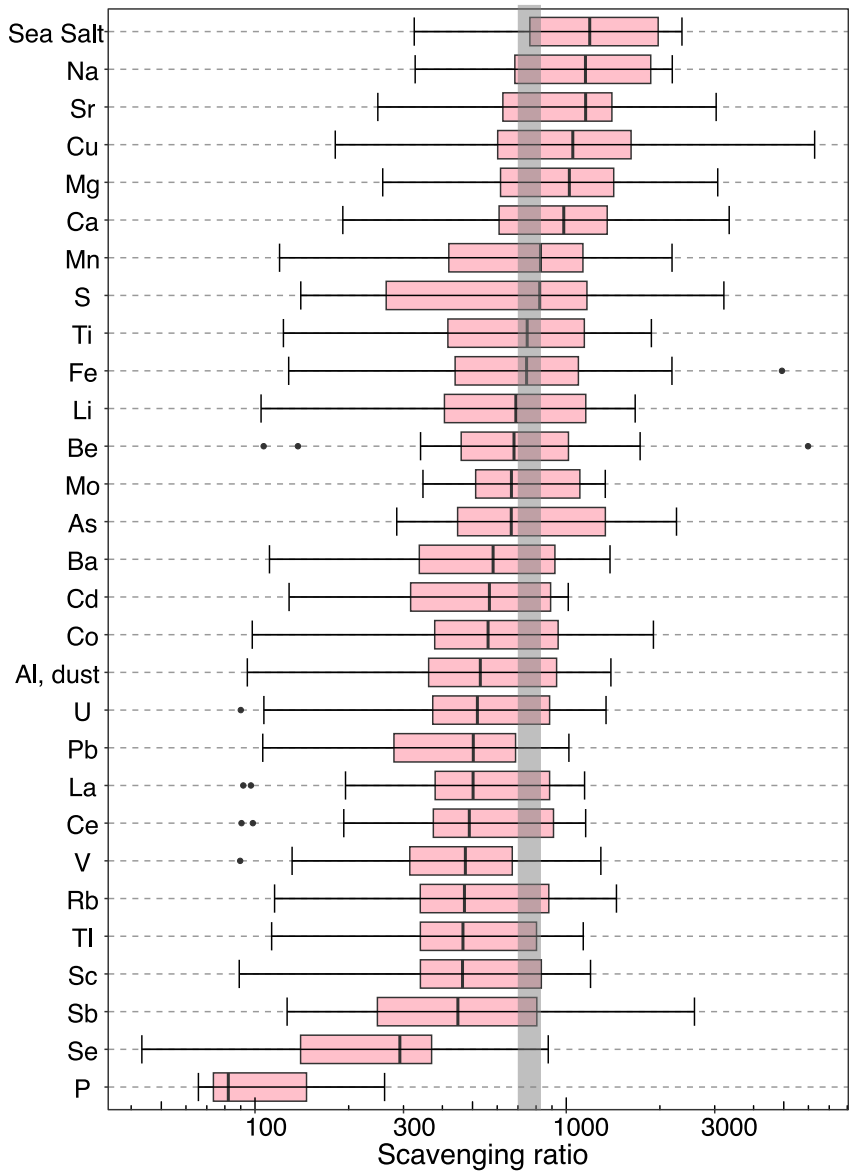

Figure 4. Scavenging ratio of elements deduced from deposition flux, aerosol concentration, and dry deposition estimates. Sample pairs with a dry deposition contribution larger than 40% are excluded. Scavenging ratio is not calculated for P and Se because estimated dry deposition is always larger than 40% for these elements. The model scavenging ratio is figured by the gray band.

are more enriched in total deposition samples than in aerosols, while crustal elements are more enriched in aerosol samples than in total deposition samples. This compositional shift exactly reflects the observed scavenging ratio variations. The elements with the highest scavenging ratio are enriched in the deposition samples, while the elements with the lowest scavenging ratio, such as Se, are depleted.

A second perturbation diagram is calculated and plotted for REEs, showing that REE profiles are not perturbed between paired aerosol and deposition samples (Figure 6). Aerosols cannot be differentiated from deposition in the REE profiles. This result implies that the dust deposition process did not lead to a shift in REE composition.

3.6. Lead Isotope Differences Between Aerosols and Deposit

Figure 7 shows the cumulative distribution of $^{206}Pb/^{207}Pb$ isotope ratios for all the aerosol and total deposition samples. The $^{206}Pb/^{207}Pb$ ratio in the distribution of aerosol samples is less radiogenic than in the distribution of

Table 1
Comparison Between Model Output and Measured Results

Parameters	Model output	Measured
Precipitation rate (mm day^{-1})	1.30	5.45
Dust scavenging ratio	750 (400–1,000)	513 (geometric mean)
Dust lifetime (day)	0.171	0.034 (median)
Dust dry deposition velocity (cm s^{-1})	0.3	0.3 (using the model value)
Dust deposition velocity (cm s^{-1})	–	2.6 (median)
Dust surface concentration (μg m^{-3})	24.5	9.6 (weighted mean)
Dust dry deposition flux (μg m^{-2} day^{-1})	9,500	2,500 (weighted mean)
Dust wet deposition flux (μg m^{-2} day^{-1})	2,070	20,990 (weighted mean)
Dust total deposition flux (μg m^{-2} day^{-1})	11,580	23,490 (weighted mean)
Sea salt scavenging ratio	750 (400–1,000)	1,080 (geometric mean)
Sea salt lifetime (day)	0.165	0.013 (median)
Sea salt dry deposition velocity (cm s^{-1})	0.3	0.3 (using the model value)
Sea salt deposition velocity (cm s^{-1})	–	6.0 (median)
Sea salt surface concentration (μg m^{-3})	13.47	9.29 (weighted mean)
Sea salt dry deposition flux (μg m^{-2} day^{-1})	5,600	2,400 (weighted mean)
Sea salt wet deposition flux (μg m^{-2} day^{-1})	985	50,700 (weighted mean)
Sea salt total deposition flux (μg m^{-2} day^{-1})	6,580	53,100 (weighted mean)

the total deposition samples, and thus more anthropogenic. An exact two-sample Mann-Whitney test calculated with R software (R Core Team, 2018) provides evidence of this visual observation, giving a p-value of 0.0005 for the hypothesis that the $^{206}Pb/^{207}Pb$ isotopic ratio is greater in the total deposition than in the aerosol. Therefore the aerosol is more anthropogenic than the total deposition in the lower atmospheric layer. This result could be due to

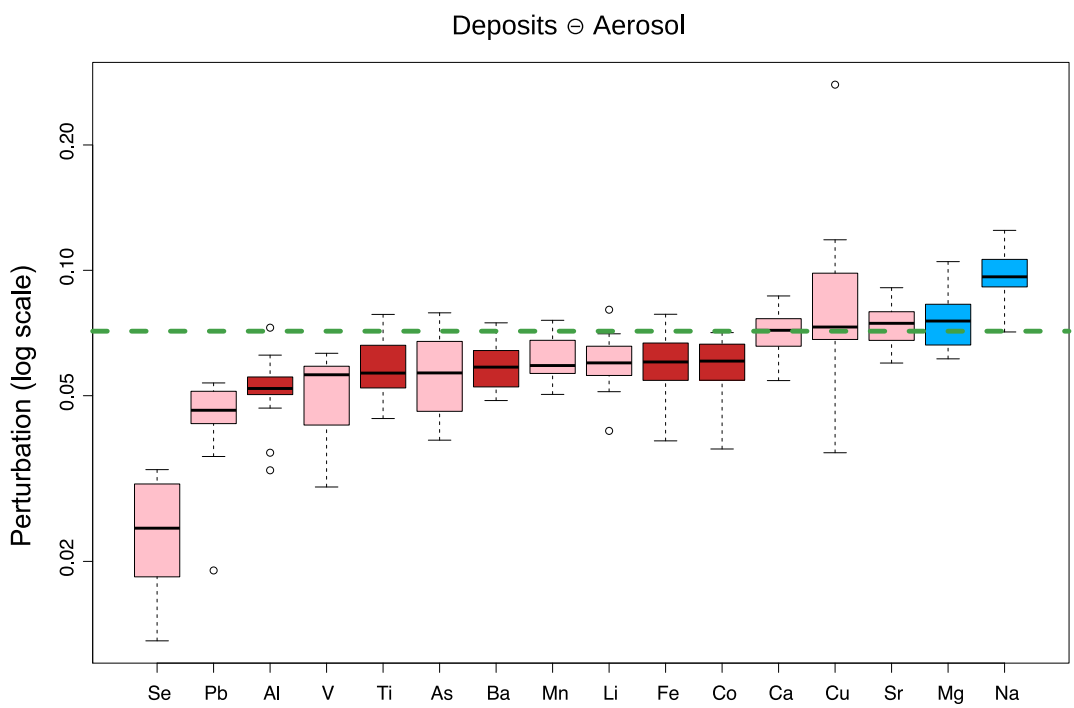

Figure 5. Perturbation diagram for trace elements. The dashed green horizontal line represents zero perturbation (no disturbance). Marine elements are indicated in blue, crustal elements in red, and other elements in pink.

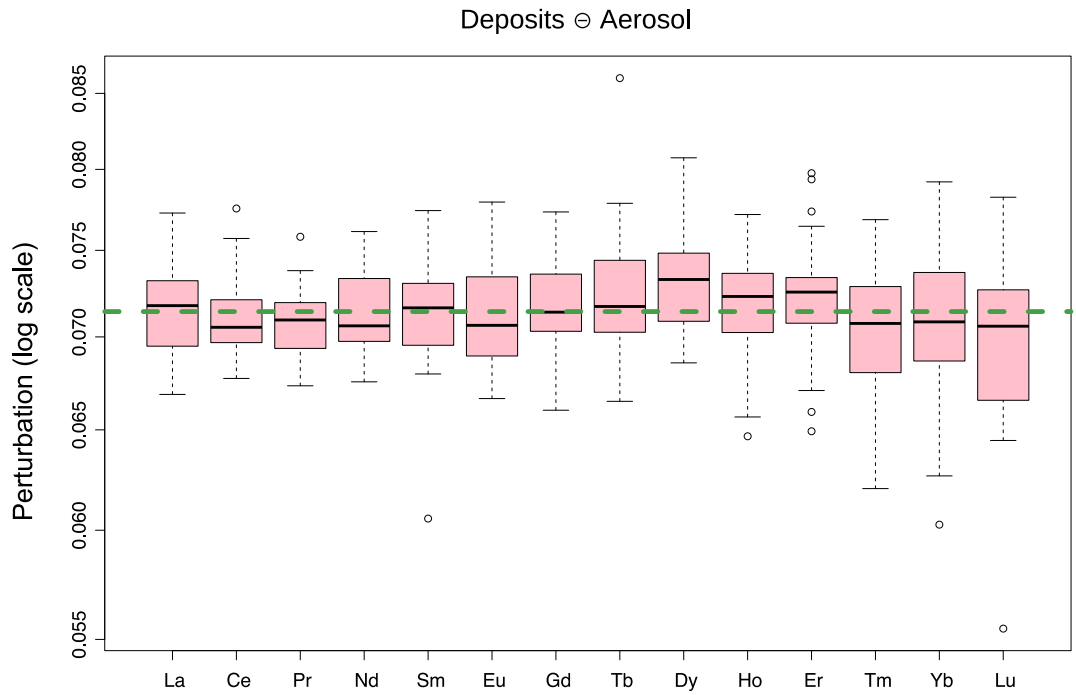

Figure 6. Perturbation diagram of Rare Earth Element profiles. The dashed green horizontal line represents zero perturbation (no disturbance).

a lower deposition velocity and scavenging ratio for anthropogenic lead, which has a larger fraction in fine mode than natural lead. This difference could also be attributed to the vertical heterogeneity of lead in aerosols, with an enrichment in anthropogenic lead locally emitted in the lower atmospheric layer.

4. Conclusion

Over the Guadeloupe Islands, total deposition fluxes are not proportionally correlated with surface aerosol concentration, and the elemental composition of atmospheric deposition is not the same as the atmospheric aerosol composition measured near ground level. Different lifetimes are observed for dust and sea-salt aerosols. This result suggests that aerosol concentration gradients may exist between the measurement location at ground level, and locations at higher altitudes in the atmosphere, where aerosols are incorporated into precipitation.

Thermal and orographic forcing may generate microscale atmospheric circulation, resulting in the enhanced vertical movement of air, high cloudiness, and higher precipitation rate compared to the nearby open ocean. The result may be the more efficient washout of suspended aerosols by wet deposition, which is not well captured by global aerosol models. Values used in models or median values measured in this study for event-dependent parameters are not appropriate to estimate deposition flux during single events or short periods. Averaged scavenging ratio values highlight a more efficient washout of locally emitted sea-salt aerosols compared to long-range transported Saharan dust and anthropogenic aerosols. Consequently, when compared to suspended aerosols, total deposition samples are more enriched in elements of marine origin and less enriched in anthropogenic lead. The REE composition is found to be the same in total deposition and aerosol samples, implying that both the deposited and suspended dust aerosol particles have the same origin and that deposition processes do not change REE composition.

Parameters often used by global models to study aerosol deposition, such as deposition velocity, lifetime, and scavenging ratio were measured and tested during the current study. The median values of these parameters measured in the Guadeloupe Islands are in good agreement with values used by global models, and can therefore be used in long-term studies to estimate the deposition flux of aerosols for long periods, if precipitation rate and surface aerosol concentration are correctly assessed. However, both aerosol concentration and precipitation rate are not well assessed by the model for the sampling site presented here. As wet deposition is found to be the main

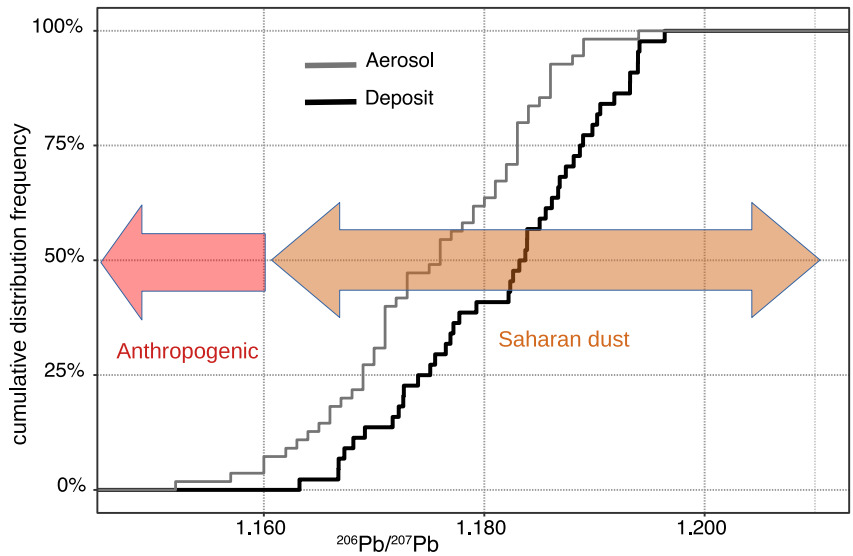

Figure 7. Cumulative distributions of lead isotope ratios $^{206}Pb/^{207}Pb$ for aerosol and deposition samples. The lead isotope ratios of anthropogenic sources range from 1.10 to 1.16 (Bollhöfer & Rosman, 2000, 2001; Monna et al., 2000) while those from the crustal Saharan source range from 1.16 to 1.22 (Guinoiseau et al., 2022).

pathway of aerosols from atmosphere to ocean and tropical island, as previously shown by Van Der Does et al. (2020), an underestimation of the total deposition flux for sea salt as well as for dust is observed in model outputs. This result is caused by the underestimation of wet deposition velocity in the model.

More comprehensive observational data from field sampling at different locations in the Caribbean region, including precipitation rates, vertical profiles, and the separation of dry versus wet deposition, would lead to better understanding of the specific mechanisms involved in atmospheric deposition. Similar measurements from marine environments could also further complement the observational data sets presented here.

Appendix A: Validation of Analytical Methods

A1. Detection Limits

The detection limits for both total deposition and aerosol measurements and for each element are calculated and listed in Table A1. The following blanks were prepared: laboratory blanks (27 for ICP-MS, and 23 for ICP-AES with acid attack only), 7 field blanks for aerosol samples (4 cellulose ester pristine filters and 3 polycarbonate filters, cleaned following the super-clean procedure) and 17 field blanks for deposition samples.

The 17 field blanks were used to check the memory effect of the sampling system by rinsing the funnel a second time with 50 mL of a 3% v:v HCl water solution after sampling.

A2. Validation of Analysis Method Using Geostandard Measurements

Nine finely ground geostandards (MAG-1, SCO-1, STM-1, SDC-1, BHVO-1, LKSD-2, BE-N, QLO-1, and BHVO-1 from USGS) were also prepared following the same digestion procedure as the deposition samples or aerosol samples to validate the digestion procedures. Geostandards were hand-crushed for 30 min in an agate mortar to approximate aerosol grain size. The powders produced were digested with or without the filter at the smallest amount that can be weighed, around 10 mg, to obtain a mass as close as possible to field aerosol samples. The results for recovery rate are listed in Table A2. Taking into account all the geostandards, the median value and average value of recovery rate for each element range from 80% to 120%, except for Tm (median value 79%) and Yb (median value 78%).

The perturbation diagram for REE profiles is plotted in Figure A1, showing the compositional difference between measured REE composition and the generally accepted REE composition in the literature. An application of

Table A1
Field Detection Limits (LD), PC Is Polycarbonate, CN Is Cellulose Nitrate

Elements	Al	Ba	Ca	Fe	K	Li	Mg	Mn
Method	AES	AES	AES	AES	Flame	AES	AES	AES
LD deposition μg m^2 day^{-1}	35	2	204	16	69	0.01	11	0.3
LD aerosol (PC) ng m^{-3}	4.1	0.1	15	2.3	824	0.01	6.5	0.04
LD aerosol (CN) ng m^{-3}	2.5	0.2	24	3.5	518	0.01	2.3	0.1
Elements	Na	P	S	Sc	Sr	Ti	Zn	Be
Method	Flame	AES	AES	AES	AES	AES	AES	MS (LR)
LD deposition μg m^2 day^{-1}	54	48	14	0.05	0.12	9.03	1.15	0.002
LD aerosol (PC) ng m^{-3}	721	67	25.6	0.03	0.1	0.1	0.7	0.002
LD aerosol (CN) ng m^{-3}	274	76	308.6	0.03	0.1	0.7	2.4	0.002
Elements	Rb	Mo	Cd	Sb	Tl	Pb	U	V
Method	MS (LR)	MS (LR)	MS (LR)	MS (LR)	MS (LR)	MS (LR)	MS (LR)	MS (MR)
LD deposition μg m^2 day^{-1}	0.039	0.05	0.005	0.074	0.0004	0.051	0.003	0.06
LD aerosol (PC) ng m^{-3}	0.155	0.054	0.006	0.309	0.000	0.027	0.003	0.009
LD aerosol (CN) ng m^{-3}	0.066	0.007	0.001	0.010	0.0001	0.009	0.003	0.05
Elements	Cr	Co	Ni	Cu	As	Se	La	Ce
Method	MS (MR)	MS (MR)	MS (MR)	MS (MR)	MS (HR)	MS (HR)	MS (HR)	MS (HR)
LD deposition μg m^2 day^{-1}	0.1	0.02	0.009	0.7	0.1	0.01	0.03	0.08
LD aerosol (PC) ng m^{-3}	0.1	0.005	0.008	0.04	0.01	0.01	0.002	0.004
LD aerosol (CN) ng m^{-3}	3	0.009	0.6	0.1	0.008	0.006	0.001	0.002
Elements	Pr	Nd	Sm	Eu	Gd	Tb	Dy	Ho
Method	MS (HR)	MS (HR)	MS (HR)	MS (HR)	MS (HR)	MS (HR)	MS (HR)	MS (HR)
LD deposition μg m^2 day^{-1}	0.01	0.04	0.01	0.002	0.008	0.002	0.007	0.001
LD aerosol (PC) ng m^{-3}	0.0005	0.001	0.001	0.00002	0.0004	0.00001	0.0003	0.00002
LD aerosol (CN) ng m^{-3}	0.0004	0.002	0.0003	0.0001	0.0003	0.00005	0.0004	0.00007
Elements	Er	Tm	Yb	Lu				
Method	MS (HR)	MS (HR)	MS (HR)	MS (HR)				
LD deposition μg m^2 day^{-1}	0.003	0.001	0.003	0.0004				
LD aerosol (PC) ng m^{-3}	0.0001	0.0001	0.0002	0.00002				
LD aerosol (CN) ng m^{-3}	0.0001	0.009	0.0002	0.00002				

Table A2
Median Recovery Rates of Geostandard Measurements: 4 MAG-1[a] Samples, 6 SCO-1[a] Samples, SDC-1[a], STM-1[a], 3 BHVO-1[a] Samples, BE-N[b,h], LKSD-2[b,g,i,j], QLO-1[a], SLRS-4[c], SLRS-5[d,e], and SLRS-6[f]

Elements	Al	Ba	Ca	Fe	K	Li	Mg	Mn
Method	AES	AES	AES	AES	Flame	AES	AES	AES
Median RR	90%	94%	93%	91%	103%	132%	94%	100%
Elements	Na	P	S	Sc	Sr	Ti	Zn	Be
Method	Flame	AES	AES	AES	AES	AES	AES	MS (LR)
Median RR	105%	109%	96%	102%	90%	86%	107%	94%
Elements	Rb	Mo	Cd	Sb	Tl	Pb	U	V
Method	MS (LR)	MS (LR)	MS (LR)	MS (LR)	MS (LR)	MS (LR)	MS (LR)	MS (MR)

Table A2
Continued

Median RR	101%	83%	132%	91%	98%	87%	97%	114%
Elements	Cr	Co	Ni	Cu	As	Se	La	Ce
Method	MS (MR)	MS (MR)	MS (MR)	MS (MR)	MS (HR)	MS (HR)	MS (HR)	MS (HR)
Median RR	101%	121%	116%	100%	102%	89%	98%	102%
Elements	Pr	Nd	Sm	Eu	Gd	Tb	Dy	Ho
Method	MS (HR)	MS (HR)	MS (HR)	MS (HR)	MS (HR)	MS (HR)	MS (HR)	MS (HR)
Median RR	105%	104%	99%	95%	98%	81%	83%	80%
Elements	Er	Tm	Yb	Lu				
Method	MS (HR)	MS (HR)	MS (HR)	MS (HR)				
Median RR	80%	79%	78%	80%				

[a]Gladney and Roelandts (1988). [b]Govindaraju (1994). [c]Yeghicheyan et al. (2001). [d]Yeghicheyan et al. (2013). [e]Heimburger et al. (2013). [f]Yeghicheyan et al. (2019). [g]Shaheen and Fryer (2011). [h]Jochum et al. (2016). [i]Hall and Pelchat (1997). [j]Leybourne et al. (2007).

compositional data analysis using perturbation diagrams is presented in Xu-Yang et al. (2021). A systematic shift can be observed between measured values and expected values. This discrepancy could be explained by the fact that we used a high-resolution ICP-MS (Element II), which eliminated for example, the polyatomic interferences of $^{141}Pr^{16}O^{+}$ or $^{138}Ba^{16}O^{+}$, $^{150}Nd^{16}O^{+}$, $^{150}Sm^{16}O^{+}$, $^{157}Gd^{16}O^{+}$, $^{159}Tb^{16}O^{+}$ on the measurement of ^{157}Gd, ^{166}Er, ^{173}Yb, and ^{175}Lu.

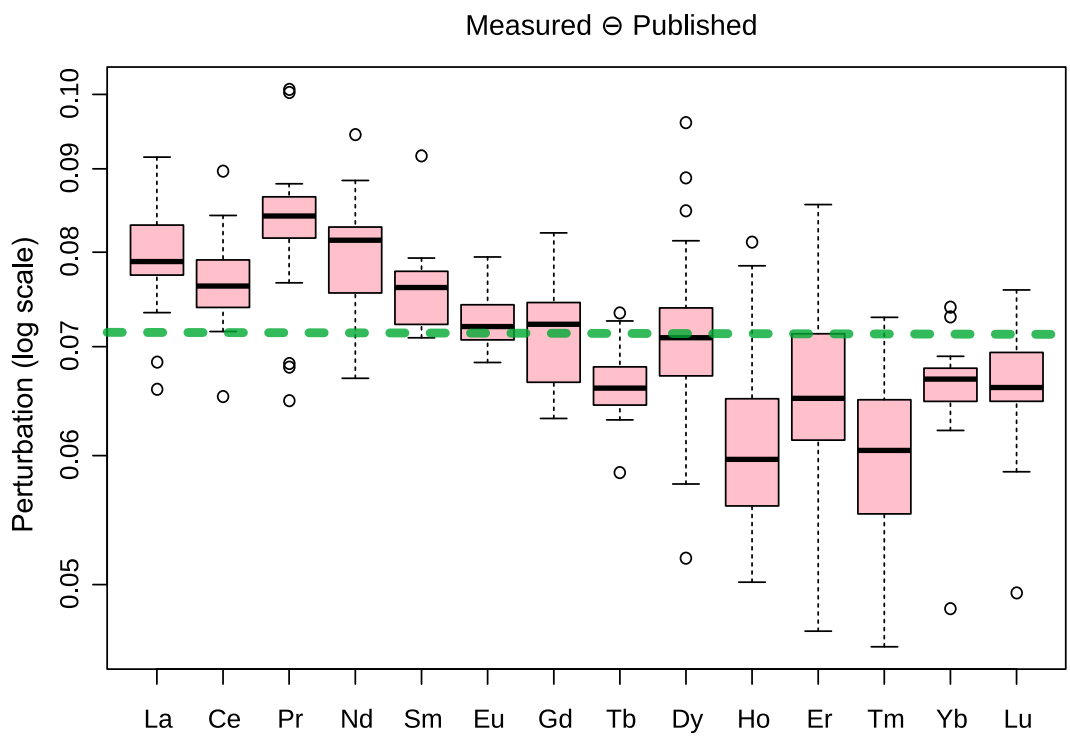

Figure A1. Measured ⊖ published values of Rare Earth Elements (REEs) (n = 18). The dashed green horizontal line represents no disturbance. The REE theoretical values come from Gladney and Roelandts (1988) for MAG-1, SCo-1, SDC-1, STM-1, BHVO-1, and QLO-1; from Govindaraju (1994) for LKSD-2 and BE-N. In LKSD-2, values of Pr, Gd, Ho, Er, and Tm come from Shaheen and Fryer (2011) because these values are absent from Govindaraju (1994).

Table A3
Validation of Pb Isotope Ratio ($^{207}Pb/^{206}Pb$)

Geostandard	MAG-1[a]	STM-1[b]
Measured $^{207}Pb/^{206}Pb$	0.829	0.799
Published $^{207}Pb/^{206}Pb$	0.830	0.801

[a]Nagender Nath et al. (2009). [b]Weis et al. (2005).

A3. Validation of Lead Isotope Ratio Measurements

Two geostandards (MAG-1 and STM-1) were analyzed in the same way as the samples to check the lead isotope ratio measurements. Results are reported in Table A3, showing good accuracy for the $^{207}Pb/^{206}Pb$ measurements presented here.

Data Availability Statement

Data are available as Open License 2.0 at https://doi.org/10.18715/IPGP.2024.m23iz47t (Losno et al., 2025).

Acknowledgments
We sincerely thank the reviewers (Jan-Berend Stuut and Anonymous) for their constructive comments. We thank the OVSG staff (Vincent Robert and Joanny Pierre) for their help in the field. Parts of this work (ICP-OES and FS-HR-ICP-MS analyses) were supported by the IPGP multidisciplinary program PARI, and by the Paris–IdF region SESAME Grant 12015908. We thank Carmela Chateau-Smith for her help with English proofreading.

References

Abouchami, W., Näthe, K., Kumar, A., Galer, S. J., Jochum, K. P., Williams, E., et al. (2013). Geochemical and isotopic characterization of the Bodélé depression dust source and implications for transatlantic dust transport to the Amazon Basin. *Earth and Planetary Science Letters*, *380*, 112–123. https://doi.org/10.1016/j.epsl.2013.08.028

Aitchison, J. (1982). The statistical analysis of compositional data. *Journal of the Royal Statistical Society: Series B*, *44*(2), 139–160. https://doi.org/10.1111/j.2517-6161.1982.tb01195.x

Aitchison, J. (1986). *The statistical analysis of compositional data*. Chapman & Hall.

Albani, S., Mahowald, N. M., Perry, A. T., Scanza, R. A., Zender, C. S., Heavens, N. G., et al. (2014). Improved dust representation in the community atmosphere model. *Journal of Advances in Modeling Earth Systems*, *6*(3), 541–570. https://doi.org/10.1002/2013MS000279

Amouroux, D., Liss, P. S., Tessier, E., Hamren-Larsson, M., & Donard, O. F. (2001). Role of oceans as biogenic sources of selenium. *Earth and Planetary Science Letters*, *189*(3–4), 277–283. https://doi.org/10.1016/S0012-821X(01)00370-3

Beaudoing, H., & Rodell, M., & NASA/GSFC/HSL. (2020). *GLDAS Noah land surface model L4 monthly 0.25 x 0.25 degree, version 2.1*. NASA Goddard Earth Sciences Data and Information Services Center. https://doi.org/10.5067/SXAVCZFAQLNO

Bellouin, N., Quaas, J., Gryspeerdt, E., Kinne, S., Stier, P., Watson-Parris, D., et al. (2020). Bounding global aerosol radiative forcing of climate change. *Reviews of Geophysics*, *58*(1), e2019RG000660. https://doi.org/10.1029/2019RG000660

Bollhöfer, A., & Rosman, K. (2000). Isotopic source signatures for atmospheric lead: The Southern Hemisphere. *Geochimica et Cosmochimica Acta*, *64*(19), 3251–3262. https://doi.org/10.1016/S0016-7037(00)00436-1

Bollhöfer, A., & Rosman, K. (2001). Isotopic source signatures for atmospheric lead: The Northern Hemisphere. *Geochimica et Cosmochimica Acta*, *65*(11), 1727–1740. https://doi.org/10.1016/S0016-7037(00)00630-X

Brewer, G. P. (1975). Minor elements in seawater. *Chemical Oceanography*, *1*, 415–496. Retrieved from https://cir.nii.ac.jp/crid/1572261549634550912

Brodsky, H., Calderón, R., Hamilton, D. S., Li, L., Miles, A., Pavlick, R., et al. (2023). Assessing long-distance atmospheric transport of soilborne plant pathogens. *Environmental Research Letters*, *18*(10), 104021. https://doi.org/10.1088/1748-9326/acf50c

Cécé, R., Bernard, D., d' Christophe, A., & Dorville, J.-F. (2014). Numerical simulations of island-induced circulations and Windward Katabatic flow over the Guadeloupe Archipelago. *Monthly Weather Review*, *142*(2), 850–867. https://doi.org/10.1175/MWR-D-13-00119.1

Chadwick, O. A., Derry, L. A., Vitousek, P. M., Huebert, B. J., & Hedin, L. O. (1999). Changing sources of nutrients during four million years of ecosystem development. *Nature*, *397*(6719), 491–497. https://doi.org/10.1038/17276

Chaperon, P., L'Hôte, Y., & Vuillaume, G. (1985). *Les ressources en eau de surface de la Guadeloupe (No. 7)*. Éd. de l'ORSTOM.

Cheng, I., Al Mamun, A., & Zhang, L. (2021). A synthesis review on atmospheric wet deposition of particulate elements: Scavenging ratios, solubility, and flux measurements. *Environmental Reviews*, *29*(3), 340–353. https://doi.org/10.1139/er-2020-0118

Cipolloni, O.-A., Couture, P., Cordonnier, S., & Pascal, P.-Y. (2024). Temporal fluctuation of metallic trace elements concentrations in three morphotypes of floating holopelagic Sargassum from the Caribbean coast (Guadeloupe, French West Indies). *Marine Pollution Bulletin*, *201*, 116229. https://doi.org/10.1016/j.marpolbul.2024.116229

Danabasoglu, G., Lamarque, J., Bacmeister, J., Bailey, D. A., DuVivier, A. K., Edwards, J., et al. (2020). The community earth system model version 2 (CESM2). *Journal of Advances in Modeling Earth Systems*, *12*(2), e2019MS001916. https://doi.org/10.1029/2019MS001916

Dassié, E. P., Gourves, P.-Y., Cipolloni, O., Pascal, P.-Y., & Baudrimont, M. (2022). First assessment of Atlantic open ocean Sargassum spp. metal and metalloid concentrations. *Environmental Science and Pollution Research*, *29*(12), 17606–17616. https://doi.org/10.1007/s11356-021-17047-8

Dessert, C., Clergue, C., Rousteau, A., Crispi, O., & Benedetti, M. F. (2020). Atmospheric contribution to cations cycling in highly weathered catchment, Guadeloupe (Lesser Antilles). *Chemical Geology*, *531*, 119354. https://doi.org/10.1016/j.chemgeo.2019.119354

Dessert, C., Lajeunesse, E., Lloret, E., Clergue, C., Crispi, O., Gorge, C., & Quidelleur, X. (2015). Controls on chemical weathering on a mountainous volcanic tropical island: Guadeloupe (French West Indies). *Geochimica et Cosmochimica Acta*, *171*, 216–237. https://doi.org/10.1016/j.gca.2015.09.009

Dong, K., Woo, C., & Yamamoto, N. (2019). Plant assemblages in atmospheric deposition. *Atmospheric Chemistry and Physics*, *19*(18), 11969–11983. https://doi.org/10.5194/acp-19-11969-2019

Duce, R. A., Liss, P. S., Merrill, J. T., Atlas, E. L., Buat-Menard, P., Hicks, B. B., et al. (1991). The atmospheric input of trace species to the world ocean. *Global Biogeochemical Cycles*, *5*(3), 193–259. https://doi.org/10.1029/91GB01778

Dulac, F., Chazette, P., Gomes, L., Chatenet, B., Berger, H., & Vinicula Dos Santos, J. (2001). A method for aerosol profiling in the lower troposphere with coupled scatter and meteorological rawindsondes and first data from the tropical Atlantic off Sahara. *Journal of Aerosol Science*, *32*(9), 1069–1086. https://doi.org/10.1016/S0021-8502(01)00043-X

Galloway, J., Savoie, D., Keene, W., & Prospero, J. (1993). The temporal and spatial variability of scavenging ratios for NSS sulfate, nitrate, methanesulfonate and sodium in the Atmosphere over the North Atlantic Ocean. Atmospheric Environment. Part A. *General Topics*, *27*(2), 235–250. https://doi.org/10.1016/0960-1686(93)90354-2

Giardina, M., & Buffa, P. (2018). A new approach for modeling dry deposition velocity of particles. *Atmospheric Environment*, *180*, 11–22. https://doi.org/10.1016/j.atmosenv.2018.02.038

Gladney, E. S., & Roelandts, I. (1988). 1987 compilation of elemental concentration data for USGS BHVO-1, MAG-1, QLO-1, RGM-1, SCo-1, SDC-1, SGR-1 and STM-1. *Geostandards and Geoanalytical Research*, *12*(2), 253–362. https://doi.org/10.1111/j.1751-908X.1988.tb00053.x

Govindaraju, K. (1994). 1994 compilation of working values and sample description for 383 geostandards. *Geostandards and Geoanalytical Research*, *18*(S1), 1–158. https://doi.org/10.1046/j.1365-2494.1998.53202081.x-i1

Groß, S., Gasteiger, J., Freudenthaler, V., Müller, T., Sauer, D., Toledano, C., & Ansmann, A. (2016). Saharan dust contribution to the Caribbean summertime boundary layer –a lidar study during SALTRACE. *Atmospheric Chemistry and Physics*, *16*(18), 11535–11546. https://doi.org/10.5194/acp-16-11535-2016

Guerreiro, C. V., Baumann, K.-H., Brummer, G.-J. A., Fischer, G., Korte, L. F., Merkel, U., et al. (2017). Coccolithophore fluxes in the open tropical North Atlantic: Influence of thermocline depth, Amazon water, and Saharan dust. *Biogeosciences*, *14*(20), 4577–4599. https://doi.org/10.5194/bg-14-4577-2017

Guerreiro, C. V., Ferreira, A., Cros, L., Stuut, J.-B., Baker, A., Tracana, A., et al. (2023). Response of coccolithophore communities to oceanographic and atmospheric processes across the North- and Equatorial Atlantic. *Frontiers in Marine Science*, *10*, 1119488. https://doi.org/10.3389/fmars.2023.1119488

Guinoiseau, D., Singh, S., Galer, S., Abouchami, W., Bhattacharyya, R., Kandler, K., et al. (2022). Characterization of Saharan and Sahelian dust sources based on geochemical and radiogenic isotope signatures. *Quaternary Science Reviews*, *293*, 107729. https://doi.org/10.1016/j.quascirev.2022.107729

Hall, G. E. M., & Pelchat, J. (1997). Determination of As, Bi, Sb, Se and Te in Fifty Five Reference Materials by Hydride Generation ICP-MS. *Geostandards Newsletter*, *21*, 85–91. https://doi.org/10.1111/j.1751-908X.1997.tb00534.x

Heimburger, A., Losno, R., Triquet, S., Dulac, F., & Mahowald, N. M. (2012). Direct measurements of atmospheric iron, cobalt, and aluminum-derived dust deposition at Kerguelen Islands: Dust deposition at Kerguelen Islands. *Global Biogeochemical Cycles*, *26*(4), GB4016. https://doi.org/10.1029/2012GB004301

Heimburger, A., Tharaud, M., Monna, F., Losno, R., Desboeufs, K., & Nguyen, E. B. (2013). SLRS-5 elemental concentrations of thirty-three uncertified elements deduced from SLRS-5/SLRS-4 ratios. *Geostandards and Geoanalytical Research*, *37*(1), 77–85. https://doi.org/10.1111/j.1751-908X.2012.00185.x

Holben, B. N., Tanré, D., Smirnov, A., Eck, T. F., Slutsker, I., Abuhassan, N., et al. (2001). An emerging ground-based aerosol climatology: Aerosol optical depth from AERONET. *Journal of Geophysical Research*, *106*(D11), 12067–12097. https://doi.org/10.1029/2001JD900014

Huneeus, N., Boucher, O., & Chevallier, F. (2009). Simplified aerosol modeling for variational data assimilation. *Geoscientific Model Development*, *2*(2), 213–229. https://doi.org/10.5194/gmd-2-213-2009

Huneeus, N., Schulz, M., Balkanski, Y., Griesfeller, J., Prospero, J., Kinne, S., et al. (2011). Global dust model intercomparison in AeroCom phase I. *Atmospheric Chemistry and Physics*, *11*(15), 7781–7816. https://doi.org/10.5194/acp-11-7781-2011

Jickells, T. D., An, Z. S., Andersen, K. K., Baker, A. R., Bergametti, G., Brooks, N., et al. (2005). Global iron connections between desert dust, ocean biogeochemistry, and climate. *Science*, *308*(5718), 67–71. https://doi.org/10.1126/science.1105959

Jochum, K. P., Weis, U., Schwager, B., Stoll, B., Wilson, S. A., Haug, G. H., et al. (2016). Reference values following ISO guidelines for frequently requested rock reference materials. *Geostandards and Geoanalytical Research*, *40*, 333–350. https://doi.org/10.1111/j.1751-908X.2015.00392.x

Kadko, D., Landing, W. M., & Shelley, R. U. (2015). A novel tracer technique to quantify the atmospheric flux of trace elements to remote ocean regions. *Journal of Geophysical Research: Oceans*, *120*(2), 848–858. https://doi.org/10.1002/2014JC010314

Kandler, K., Schneiders, K., Ebert, M., Hartmann, M., Weinbruch, S., Prass, M., & Pöhlker, C. (2018). Composition and mixing state of atmospheric aerosols determined by electron microscopy: Method development and application to aged Saharan dust deposition in the Caribbean boundary layer. *Atmospheric Chemistry and Physics*, *18*(18), 13429–13455. https://doi.org/10.5194/acp-18-13429-2018

Kennedy, M. J., Chadwick, O. A., Vitousek, P. M., Derry, L. A., & Hendricks, D. M. (1998). Changing sources of base cations during ecosystem development, Hawaiian Islands. *Geology*, *26*(11), 1015. https://doi.org/10.1130/0091-7613(1998)026⟨1015:CSOBCD⟩2.3.CO;2

Klug, W. & Communities, C. O. T. E. (Eds.) (1992)., *Evaluation of long range atmospheric transport models using environmental radioactivity data from the Chernobyl accident: The ATMES report*. Elsevier Applied Science.

Kok, J. F., Mahowald, N. M., Fratini, G., Gillies, J. A., Ishizuka, M., Leys, J. F., et al. (2014). An improved dust emission model – Part 1: Model description and comparison against measurements. *Atmospheric Chemistry and Physics*, *14*(23), 13023–13041. https://doi.org/10.5194/acp-14-13023-2014

Korte, L. F., Brummer, G. A., Van Der Does, M., Guerreiro, C. V., Mienis, F., Munday, C. I., et al. (2020). Multiple drivers of production and particle export in the western tropical North Atlantic. *Limnology & Oceanography*, *65*(9), 2108–2124. https://doi.org/10.1002/lno.11442

Korte, L. F., Brummer, G.-J., Van Der Does, M., Guerreiro, C. V., Hennekam, R., Van Hateren, J. A., et al. (2016). Compositional changes of present-day transatlantic Saharan dust deposition. https://doi.org/10.5194/acp-2016-1068

Korte, L. F., Brummer, G.-J. A., Van Der Does, M., Guerreiro, C. V., Hennekam, R., Van Hateren, J. A., et al. (2017). Downward particle fluxes of biogenic matter and Saharan dust across the equatorial North Atlantic. *Atmospheric Chemistry and Physics*, *17*(9), 6023–6040. https://doi.org/10.5194/acp-17-6023-2017

Kulshrestha, U., Reddy, L., Satyanarayana, J., & Kulshrestha, M. J. (2009). Real-time wet scavenging of major chemical constituents of aerosols and role of rain intensity in Indian region. *Atmospheric Environment*, *43*(32), 5123–5127. https://doi.org/10.1016/j.atmosenv.2009.07.025

Leybourne, M. I., Denison, R. E., Cousens, B. L., Bezys, R. K., Gregoire, D. C., Boyle, D. R., et al. (2007). Geochemistry, geology, and isotopic (Sr, S, and B) composition of evaporites in the Lake St. Martin impact structure: New constraints on the age of melt rock formation. *Geochemistry, Geophysics, Geosystems*, *8*, 2006GC001481. https://doi.org/10.1029/2006GC001481

Li, J., Wang, X., Chen, J., Zhu, C., Li, W., Li, C., et al. (2017). Chemical composition and droplet size distribution of cloud at the summit of Mount Tai, China. *Atmospheric Chemistry and Physics*, *17*(16), 9885–9896. https://doi.org/10.5194/acp-17-9885-2017

Li, L., Mahowald, N. M., Kok, J. F., Liu, X., Wu, M., Leung, D. M., et al. (2022). Importance of different parameterization changes for the updated dust cycle modeling in the Community Atmosphere Model (version 6.1). *Geoscientific Model Development*, *15*(22), 8181–8219. https://doi.org/10.5194/gmd-15-8181-2022

Liu, X., Easter, R. C., Ghan, S. J., Zaveri, R., Rasch, P., Shi, X., et al. (2012). Toward a minimal representation of aerosols in climate models: Description and evaluation in the community atmosphere model CAM5. *Geoscientific Model Development*, *5*(3), 709–739. https://doi.org/10.5194/gmd-5-709-2012

Liu, X., Ma, P.-L., Wang, H., Tilmes, S., Singh, B., Easter, R. C., et al. (2016). Description and evaluation of a new four-mode version of the modal aerosol module (MAM4) within version 5.3 of the community atmosphere model. *Geoscientific Model Development*, *9*(2), 505–522. https://doi.org/10.5194/gmd-9-505-2016

Losno, R., Xu-Yang, Y., & Dessert, C. (2025). *Replication data for: Atmospheric aerosols versus total atmospheric deposition in Guadeloupe (Lesser Antilles): Composition, concentration, and fluxatmospheric aerosols versus total atmospheric deposition in Guadeloupe (Lesser Antilles): Composition, concentration, and flux [Dataverse tables]*. IPGP Research Collection. https://doi.org/10.18715/IPGP.2024.m23iz47t

Luo, C., Mahowald, N. M., & Del Corral, J. (2003). Sensitivity study of meteorological parameters on mineral aerosol mobilization, transport, and distribution. *Journal of Geophysical Research*, *108*(D15), 2003JD003483. https://doi.org/10.1029/2003JD003483

Mahowald, N. M., Albani, S., Kok, J. F., Engelstaeder, S., Scanza, R., Ward, D. S., & Flanner, M. G. (2014). The size distribution of desert dust aerosols and its impact on the Earth system. *Aeolian Research*, *15*, 53–71. https://doi.org/10.1016/j.aeolia.2013.09.002

Mahowald, N. M., Li, L., Vira, J., Prank, M., Hamilton, D. S., Matsui, H., et al. (2024). AERO-MAP: A data compilation and modelling approach to understand the fine and coarse mode aerosol composition (preprint). *ESSD – Atmosphere/Atmospheric chemistry and physics*. https://doi.org/10.5194/essd-2024-1

Mahowald, N. M., Muhs, D. R., Levis, S., Rasch, P. J., Yoshioka, M., Zender, C. S., & Luo, C. (2006). Change in atmospheric mineral aerosols in response to climate: Last glacial period, preindustrial, modern, and doubled carbon dioxide climates: DUST response to climate. *Journal of Geophysical Research*, *111*(D10), D10202. https://doi.org/10.1029/2005JD006653

Mahowald, N. M., Ward, D. S., Kloster, S., Flanner, M. G., Heald, C. L., Heavens, N. G., et al. (2011). Aerosol impacts on climate and biogeochemistry. *Annual Review of Environment and Resources*, *36*(1), 45–74. https://doi.org/10.1146/annurev-environ-042009-094507

McClintock, M., Brocard, G., Willenbring, J., Tamayo, C., Porder, S., & Pett-Ridge, J. (2015). Spatial variability of African dust in soils in a montane tropical landscape in Puerto Rico. *Chemical Geology*, *412*, 69–81. https://doi.org/10.1016/j.chemgeo.2015.06.032

McClintock, M., McDowell, W., González, G., Schulz, M., & Pett-Ridge, J. (2019). African dust deposition in Puerto Rico: Analysis of a 20-year rainfall chemistry record and comparison with models. *Atmospheric Environment*, *216*, 116907. https://doi.org/10.1016/j.atmosenv.2019.116907

Monna, F., Clauer, N., Toulkeridis, T., & Lancelot, J. (2000). Influence of anthropogenic activity on the lead isotope signature of Thau Lake sediments (southern France): Origin and temporal evolution. *Applied Geochemistry*, *15*(9), 1291–1305. https://doi.org/10.1016/S0883-2927(99)00117-1

Murphy, D. M., Froyd, K. D., Bian, H., Brock, C. A., Dibb, J. E., DiGangi, J. P., et al. (2019). The distribution of sea-salt aerosol in the global troposphere. *Atmospheric Chemistry and Physics*, *19*(6), 4093–4104. https://doi.org/10.5194/acp-19-4093-2019

Nagender Nath, B., Makishima, A., Noordmann, J., Tanaka, R., & Nakamura, E. (2009). Comprehensive analysis for major, minor and trace element contents and Sr-Nd-Pb-Hf isotope ratios in sediment reference materials, JSd-1 and MAG-1. *Geochemical Journal*, *43*(3), 207–216. https://doi.org/10.2343/geochemj.1.0018

Pabortsava, K., Lampitt, R. S., Benson, J., Crowe, C., McLachlan, R., Le Moigne, F. A. C., et al. (2017). Carbon sequestration in the deep Atlantic enhanced by Saharan dust. *Nature Geoscience*, *10*(3), 189–194. https://doi.org/10.1038/ngeo2899

Petroff, A., & Zhang, L. (2010). Development and validation of a size-resolved particle dry deposition scheme for application in aerosol transport models. *Geoscientific Model Development*, *3*(2), 753–769. https://doi.org/10.5194/gmd-3-753-2010

Pett-Ridge, J. C., Derry, L. A., & Barrows, J. K. (2009). Ca/Sr and $^{87}Sr/^{86}Sr$ ratios as tracers of Ca and Sr cycling in the Rio Icacos watershed, Luquillo Mountains, Puerto Rico. *Chemical Geology*, *267*(1–2), 32–45. https://doi.org/10.1016/j.chemgeo.2008.11.022

Pett-Ridge, J. C., Derry, L. A., & Kurtz, A. C. (2009). Sr isotopes as a tracer of weathering processes and dust inputs in a tropical granitoid watershed, Luquillo Mountains, Puerto Rico. *Geochimica et Cosmochimica Acta*, *73*(1), 25–43. https://doi.org/10.1016/j.gca.2008.09.032

Prospero, J. M., Landing, W. M., & Schulz, M. (2010). African dust deposition to Florida: Temporal and spatial variability and comparisons to models. *Journal of Geophysical Research*, *115*(D13), D13304. https://doi.org/10.1029/2009JD012773

Rahn, K. (1976). *The chemical composition of the atmospheric aerosol (Tech. Rep.)*. Graduate School of Oceanography, University of Rhode Island. Retrieved from https://books.google.fr/books?hl=fr&lr=&id=q-dOAQAAMAAJ&oi=fnd&pg=PA1&dq=The+Chemical+Composition+of+the+Atmospheric+Aerosol&ots=Gz11fOEivU&sig=lYh8sJjlLtUuA5KXxST6YbXU34c#v=onepage&q=The%20Chemical%20Composition%20of%20the%20Atmospheric%20Aerosol&f=false

Rasch, P. J., Collins, W. D., & Eaton, B. E. (2001). Understanding the Indian Ocean Experiment (INDOEX) aerosol distributions with an aerosol assimilation. *Journal of Geophysical Research*, *106*(D7), 7337–7355. https://doi.org/10.1029/2000JD900508

Raynor. (1974). Experimental studies of pollen deposition to vegetated surfaces. In *Atmosphere-surface exchange of particulate and gaseous pollutants (1974): Proceedings of a symposium held at Richland, Washington, September 4-6, 1974* (p. 988). United States Energy Research and Development Administration. Retrieved from https://www.osti.gov/servlets/purl/7273062#page=277

R Core Team. (2018). *R: A language and environment for statistical computing*. R Foundation for Statistical Computing. Retrieved from http://www.R-project.org/

Reid, J. S., Kinney, J. E., Westphal, D. L., Holben, B. N., Welton, E. J., Tsay, S., et al. (2003). Analysis of measurements of Saharan dust by airborne and ground-based remote sensing methods during the Puerto Rico Dust Experiment (PRIDE). *Journal of Geophysical Research*, *108*(D19), 2002JD002493. https://doi.org/10.1029/2002JD002493

Rudnick, R., & Gao, S. (2014). Composition of the continental crust. In *Treatise on geochemistry* (pp. 1–51). Elsevier. https://doi.org/10.1016/B978-0-08-095975-7.00301-6

Shaheen, M. E., & Fryer, B. J. (2011). A simple solution to expanding available reference materials for Laser Ablation Inductively Coupled Plasma Mass Spectrometry analysis: Applications to sedimentary materials. *Spectrochimica Acta Part B: Atomic Spectroscopy*, *66*(8), 627–636. https://doi.org/10.1016/j.sab.2011.06.010

Shao, Y., Wyrwoll, K.-H., Chappell, A., Huang, J., Lin, Z., McTainsh, G. H., et al. (2011). Dust cycle: An emerging core theme in Earth system science. *Aeolian Research*, *2*(4), 181–204. https://doi.org/10.1016/j.aeolia.2011.02.001

Slinn, W., Hasse, L., Hicks, B., Hogan, A., Lal, D., Liss, P., et al. (1978). Some aspects of the transfer of atmospheric trace constituents past the air-sea interface. *Atmospheric Environment*, *12*(11), 2055–2087. https://doi.org/10.1016/0004-6981(78)90163-4

Tegen, I., & Fung, I. (1994). Modeling of mineral dust in the atmosphere: Sources, transport, and optical thickness. *Journal of Geophysical Research*, *99*(D11), 22897–22914. https://doi.org/10.1029/94JD01928

Tegen, I., Harrison, S. P., Kohfeld, K., Prentice, I. C., Coe, M., & Heimann, M. (2002). Impact of vegetation and preferential source areas on global dust aerosol: Results from a model study. *Journal of Geophysical Research*, *107*(D21), AAC14-1–AAC14-27. https://doi.org/10.1029/2001JD000963

van den Boogaart, K. G., & Tolosana-Delgado, R. (2013). *Analyzing compositional data with R*. Springer.

Van Der Does, M., Brummer, G. A., Korte, L. F., & Stuut, J. W. (2021). Seasonality in Saharan dust across the Atlantic Ocean: From atmospheric transport to seafloor deposition. *Journal of Geophysical Research: Atmospheres*, *126*(11), e2021JD034614. https://doi.org/10.1029/2021JD034614

Van Der Does, M., Brummer, G. A., Van Crimpen, F. C. J., Korte, L. F., Mahowald, N. M., Merkel, U., et al. (2020). Tropical rains controlling deposition of Saharan dust across the North Atlantic Ocean. *Geophysical Research Letters*, *47*(5), e2019GL086867. https://doi.org/10.1029/2019GL086867

Van Der Does, M., Pourmand, A., Sharifi, A., & Stuut, J.-B. W. (2018). North African mineral dust across the tropical Atlantic Ocean: Insights from dust particle size, radiogenic Sr-Nd-Hf isotopes and rare earth elements (REE). *Aeolian Research*, *33*, 106–116. https://doi.org/10.1016/j.aeolia.2018.06.001

Vet, R., Artz, R. S., Carou, S., Shaw, M., Ro, C.-U., Aas, W., et al. (2014). A global assessment of precipitation chemistry and deposition of sulfur, nitrogen, sea salt, base cations, organic acids, acidity and pH, and phosphorus. *Atmospheric Environment*, *93*, 3–100. https://doi.org/10.1016/j.atmosenv.2013.10.060

Weinzierl, B., Ansmann, A., Prospero, J. M., Althausen, D., Benker, N., Chouza, F., et al. (2017). The Saharan aerosol long-range transport and aerosol–cloud-interaction experiment: Overview and selected highlights. *Bulletin of the American Meteorological Society*, *98*(7), 1427–1451. https://doi.org/10.1175/BAMS-D-15-00142.1

Weis, D., Kieffer, B., Maerschalk, C., Pretorius, W., & Barling, J. (2005). High-precision Pb-Sr-Nd-Hf isotopic characterization of USGS BHVO-1 and BHVO-2 reference materials. *Geochemistry, Geophysics, Geosystems*, *6*(2), 2004GC000852. https://doi.org/10.1029/2004GC000852

Xu-Yang, Y., Dessert, C., & Losno, R. (2022). Atmospheric deposition over the Caribbean region: Sea salt and Saharan dust are sources of essential elements on the island of Guadeloupe. *Journal of Geophysical Research: Atmospheres*, *127*(22), e2022JD037175. https://doi.org/10.1029/2022JD037175

Xu-Yang, Y., Losno, R., Monna, F., Rajot, J.-L., Labiadh, M., Bergametti, G., & Marticorena, B. (2021). Compositional data analysis (CoDA) as a tool to evaluate a new low-cost settling-based PM_{10} sampling head in a desert dust source region (preprint). *Aerosols/In Situ Measurement/Validation and Intercomparisons*. https://doi.org/10.5194/amt-2021-70

Yeghicheyan, D., Aubert, D., Bouhnik-Le Coz, M., Chmeleff, J., Delpoux, S., Djouraev, I., et al. (2019). A new interlaboratory characterisation of silicon, rare earth elements and twenty-two other trace element concentrations in the natural river water certified reference material SLRS-6 (NRC-CNRC). *Geostandards and Geoanalytical Research*, *43*, 475–496. https://doi.org/10.1111/ggr.12268

Yeghicheyan, D., Bossy, C., Bouhnik Le Coz, M., Douchet, C., Granier, G., Heimburger, A., et al. (2013). A compilation of silicon, rare earth element and twenty-one other trace element concentrations in the natural river water reference material SLRS-5 (NRC-CNRC). *Geostandards and Geoanalytical Research*, *37*, 449–467. https://doi.org/10.1111/j.1751-908X.2013.00232.x

Yeghicheyan, D., Carignan, J., Valladon, M., Le Coz, M. B., Cornec, F. L., Castrec-Rouelle, M., et al. (2001). A compilation of silicon and thirty one trace elements measured in the natural river water reference material SLRS-4 (NRC-CNRC). *Geostandards Newsletter*, *25*(2–3), 465–474. https://doi.org/10.1111/j.1751-908x.2001.tb00617.x

Yu, H., Chin, M., Yuan, T., Bian, H., Remer, L. A., Prospero, J. M., et al. (2015). The fertilizing role of African dust in the Amazon rainforest: A first multiyear assessment based on data from cloud-aerosol lidar and infrared pathfinder satellite observations: Dust deposition in the Amazon rainforest. *Geophysical Research Letters*, *42*(6), 1984–1991. https://doi.org/10.1002/2015GL063040

Zender, C. S., Bian, H., & Newman, D. (2003). Mineral dust entrainment and deposition (DEAD) model: Description and 1990s dust climatology. *Journal of Geophysical Research*, *108*(D14), 4416. https://doi.org/10.1029/2002JD002775